Introduction

Nanoparticles and nanostructural materials represent an evolving technology that has an impact on an incredibly wide number of industry and markets. Nanotechnology deals with the synthesis of materials, structures and/or devices having dimensions up to ~ 100 nm with new properties. The synthesis and characterization of nanocrystals is a very exciting emerging field of research which has received important scientific and technological attention.[(1)] A variety of supermolecular ensembles, multifunctional supermolecules, carbon nanotubes, metal and semiconductor nanoparticles,[(1)] have been synthesized and proposed as potential building blocks of optical and electronic devices.

1.1. Synthesis of Nanostructured Materials

In general, there are two approaches to nanoparticle production that are commonly referred to as 'top-down' and 'bottom-up'. 'Top-down' nanoparticles are generated from the size reduction of bulk materials. They generally rely on physical, the combination of physical and chemical, electrical or thermal processes for their production. Such methods include high-energy milling, mechano-chemical processing, electro-explosion, laser ablation, sputtering and vapour condensation.

'Bottom-up' approaches generate nanoparticles from the atomic or molecular level and thus are predominantly chemical processes. Commonly used techniques are crystallisation/precipitation, sol gel methods, chemical vapour deposition and self-assembly routes. Some processes may use a combination of both.

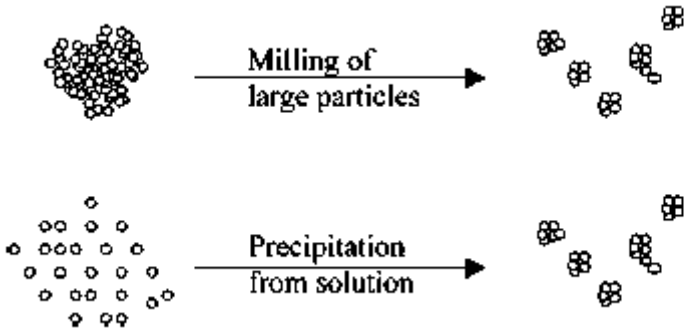

Figure 1.1: Schematic of the two general nanoparticle production techniques.

Both approaches may be performed in all three states of matter, i.e., vapour, solid or liquid (or combination of these) and the limits to the physical size of nanoparticles produced by either approach are converging and may overlap.

The choice of particle size, from a product design perspective, is directly influenced by process economics, capability to supply and the adequacy and type of performance required in the target application. Nanoparticles have a size dimension up to 100 nm and thus represent a 'bridge' between the quantum and 'real' world (micro and macro). Table 1.1 summarizes the range of production processes by type.

Table 1.1: Summary of production processes by type.

Process routes	
Top-down	Bottom-up
High-energy milling Chemical mechanical milling Vapour phase condensation Electro-explosion Laser ablation Sputtering	Crystallisation Sol-gel Chemical vapour deposition Self-assembly

1.2. Properties of Nanostructured Materials

Nanomaterial properties differ from their 'real' (bulk) counterparts primarily due to changes in physical attributes (size, shape and specific surface area) and quantum effects such as quantum confinement (the organization of energy levels into which electrons can climb or fall being squeezed into a dimension that approaches a critical quantum measurement). As a result of these nanoscale particle dimensions the properties that can change from those observed in the bulk include mechanical, physical, chemical, electronic, optical and magnetic. A change in more than one property may occur in the same particle (e.g. optical and electrical) so that particles with a range of functionalities can be engineered for target applications. Moreover, these properties may be used intentionally to directly affect bulk properties of any material system into which they are incorporated. Some examples of property changes resulting from nanoparticle dimensionality are presented below:

a) Surface activity: when the particle size of Au, for example, is reduced to 2–10 nm the catalytic activity of supported gold catalysts can be significantly enhanced.**(2)**

b) Mechanical: the hardness of silicon nanospheres (20–50 nm) has been measured to be four times greater than the expected value for bulk silicon (50 Gpa cf. 12 Gpa).**(3)**

c) Optical: nanoparticles, with dimensions less than the wavelength of light (400–700 nm), appear transparent when well dispersed. Moreover, colour and luminescent properties can be significantly altered.**(1)**

d) Electronic: the electronic structure of a nanocrystal critically depends on its size. For small particles, the electronic energy levels are not continuous as in bulk materials, but discrete, due to the confinement of the

electron wavefunction as a result of the physical dimensions of the individual nanoparticles. This confinement exhibits quantum size effects influencing properties such as electrical conductivity and magnetic susceptibility. Perhaps the most impressive example of the relationship between size and electronic

e) Magnetic: magnetic properties of nanoparticles of transition metals such as Co, Ni show marked variations with size.[(4)]

As a particle becomes smaller it theoretically can physically fit into, be assembled or positioned onto/into or pass through significantly smaller spaces. The implications of this feature are enormous in terms of the potential applications. Perhaps the greatest realised impact of this has been in the functional quality and performance properties of bulk material systems such as polymer nanocomposites and coatings (lighter, stronger, functionally smarter); ceramic composite materials (improved fracture toughness, wear resistance, greater biocompatibility, etc.); data storage and processing systems (greater capacity to store and process at reduced size); dispersions (for chemical mechanical polishing, personal care); sensors and instrumentation, drug delivery systems and enhanced activity in catalytic processes.

The nanoparticles can be fabricated in various forms depending on there uses. This can be done by:

i) **Directed assembly:** which need functionalized surface for assembly of nanoparticles into a) core-shell structures and nanocapsules

ii) **Template-based assembly:** in which templates are needed for fabrication of nanopatricles with controlled size and shape such as fabrication of nanowires and nanotubes by using templates with regular arrays of channels.

iii) **Patterned structures (2D and 3D):** in which small structures or

clusters can be generated.

1.3. Applications of Nanostructured Materials

Nanostructured materials exhibit a host of interesting new phenomena directly related to their reduced dimensionality. Not only the electronic, magnetic and optical properties but also chemical, electrochemical and catalytic properties of nanostructured materials are very different from those of the bulk form and depend sensitively on size, shape and composition.[(5)] The large surface-to-volume ratio and the variation in geometry and electronic structure have a dramatic effect on transport and catalytic properties. The range of applications is broad and growing with the current main uses as functional additives or precursors for emulsions, composites and coatings. Recently, much interest has been focused on semiconductor nanocrystals because they exhibit strongly size-dependent optical and electrical properties.

The polymer properties that show substantial performance improvements include: mechanical properties (e.g., strength, modulus and dimensional stability), decreased permeability (to gases, water and hydrocarbons), thermal and UV stability and heat distortion temperature, flame retardancy and reduced smoke emissions, chemical resistance, surface appearance, electrical conductivity and optical clarity and increased resistance to solar degradation in comparison to conventionally filled polymers. Main application areas of nanoparticles are as additives to polymers used in the transport (automotive and aerospace) sector (vehicle parts for lighter weight and higher performance), packaging (including food and biomedical) to protect and preserve the integrity of the product by controlling the barrier, mechanical, optical and respiration properties, textiles (increased strength, water resistance, self cleaning, fade resistance)

and personal care products (UV protection, deep penetration skin cream emulsions). Many of these functionalities can be interchanged from one application to another. For example, similar technology used for transparent UV protective coatings such as sunscreens in personal care. Products can be also used for UV protection in food packaging, paints, textiles, plastics used in outdoor use and protection of wood without altering the optical properties.

In the communications and information technology sectors, nanoparticles are used for increasing the efficiency of electronics by increasing the information storage capacity whilst reducing the size and weight of devices and components. Additionally, dispersions of nanoparticles in different matrices are used for chemical–mechanical planarisation (CMP) of hard drives and high surface area carbons are used in energy storage devices such as supercapacitors.[6] Other important areas include inks and ink printable electronic circuitry. The paper industry has employed nanoparticle technology for improving fillers and coatings.[7]

As can be seen from this overview, nanoparticles are being designed and delivered into a broad and ever-increasing range of applications. Nanostructures are playing a fundamental role in the advancement of biology as a result of the continuing dramatic progress in understanding the electronic, optical, and mechanical properties of an ever increasing variety of nanostructures.

There is no doubt that harnessing solar energy with inexpensive materials and manufacturing methods is one of the most important challenges facing humanity. Solar-to-electrical energy conversion methods that make use of photosensitized nanostructures are emerging as an inexpensive alternative to the p-n junction solar cell.

1.4. Titanium Oxide

1.4.1. Crystal structure

Titanium oxides are ones of the oxides which used recently in many applications. It occurs primarily in minerals like rutile, ilmenite, leucoxene, anatase, brookite, perovskite, and sphene, and it is found in titanates and many iron ores. The metal was also found in meteorites and has been detected in Sun and M-type stars. Besides the four polymorphs of TiO_2 found in nature (i.e., anatase (tetragonal), brookite (orthorhombic), rutile (tetragonal), and TiO_2 (B) (monoclinic)), two additional high-pressure forms have been synthesized starting from rutile: TiO_2(II),[8] which has the PbO_2 structure, and TiO_2(H)[9] with the hollandite structure. The structures of rutile, anatase and brookite can be discussed in terms of (TiO_2^{-6}) octahedrals. The three crystal structures differ by the distortion of each octahedral and by the assembly patterns of the octahedral chains. Anatase can be regarded to be built up from octahedrals that are connected by their vertices, in rutile, the edges are connected, and in brookite, both vertices and edges are connected (Fig.1.2).

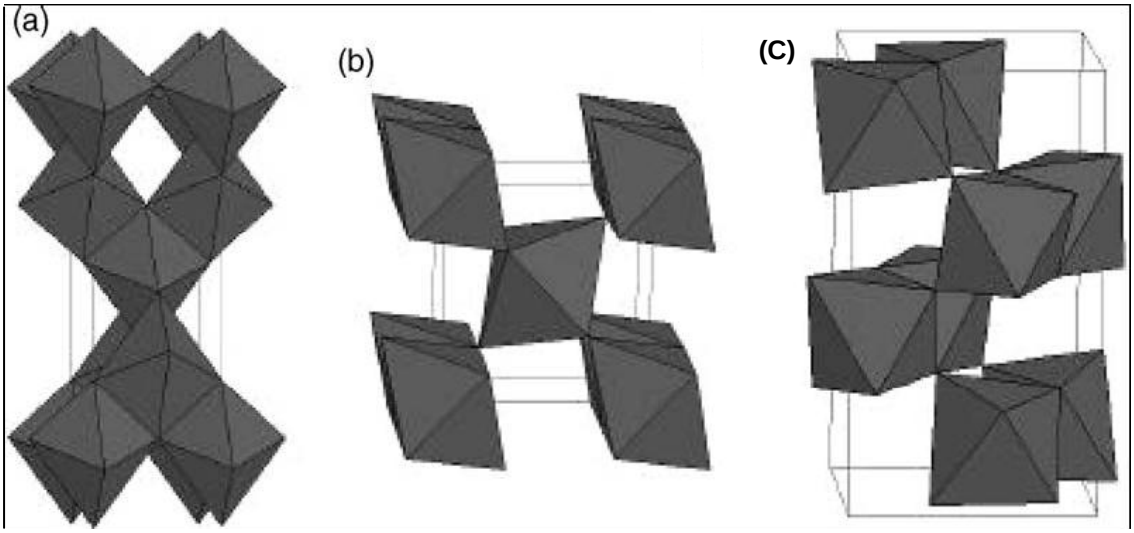

Fig. 1.2. Crystal structures of anatase (a), rutile (b), and brookite (c).

From Thermodynamic calculations rutile is the stablest phase at all temperatures and pressures up to 60 kbar.[10] The small differences in the Gibbs free energy (4–20 kJ/mole) between the three phases suggest that the metastable polymorphs are almost as stable as rutile at normal pressures and temperatures. Particle size experiments affirm that the relative phase stability may reverse when particle sizes decrease to sufficiently low values due to surface-energy effects (surface free energy and surface stress, which depend on particle size).[11] If the particle sizes of the three crystalline phases are equal, anatase is most thermodynamically stable at sizes less than 11 nm, brookite is most stable between 11 and 35 nm, and rutile is most stable at sizes greater than 35 nm.[12] This agrees with the observation that anatase is the common product of the industrial sulfate process.[13] The enthalpy of the anatase - rutile phase transformation is low. Kinetically, anatase is stable, i.e., its transformation into rutile at room temperature is so slow that the transformation practically does not occur. At macroscopic scale, the transformation reaches a measurable speed for bulk TiO_2 at T > 873 K.[14]

1.4.2. Synthesis methods

TiO_2 can be prepared in the form of powder, crystals, or thin films. Both powders and films can be built up from crystallites ranging from a few nanometers to several micrometers. It should be noted that nanosized crystallites tend to agglomerate. If separate nanosized particles are desired, often a deagglomeration step is necessary. Many novel methods lead to nanoparticles without an additional deagglomeration step.[15] Generally, TiO_2 can be prepared by two routes:

Solution route

Precipitation(co-)methods, solvothermal methods, sol–gel methods,

microemulsion methods, electrochemical synthesis and combustion synthesis.

Gas phase route :

Chemical vapour deposition (CVD), physical vapour deposition (PVD), spray pyrolysis deposition (SPD)

TiO_2 is also synthesized in special morphologies. Nanostructures especially have been built in various sizes and shapes. To complete the list, we include: nanorods, platelets, nanowires, nanowalls, nanotubes, nanoribbons, whis- kersinverse opals (ordered mesoporous materials in which air voids are surrounded by TiO_2 in a 3-D lattice), and fractals.

1.4.3. Applications :

TiO_2 has received a great deal of attention due to its chemical stability, non-toxicity, low cost, and other advantageous properties. As a result of its high refractive index, it is used as anti-reflection coating in silicon solar cells and in many thin-film optical devices.[16] TiO_2 is successfully used as gas sensor (due to the dependence of the electric conductivity on the ambient gas composition and is utilized in the determination of oxygen [17] and CO concentrations at high temperatures (> 873 K), and simultaneously determining CO/O_2 and CO/CH_4[18] concentrations. Due to its hemocompatibility with the human body, TiO_2 is used as a biomaterial (as bone substituent and reinforcing mechanical supports). TiO_2 is also used in catalytic reactions acting as a promoter, a carrier for metals and metal oxides, an additive, or as a photocatalyst. Catalysts commonly employed in the process promote pollutant destruction when illuminated with ultraviolet (UV) light.[19] A heterogeneous photocatalytic system consists of semiconductor particles (photocatalyst), which are in close contact with a liquid or gaseous reaction medium. Exposing the catalyst to light excited states are generated,

which are able to initiate subsequent processes like redox reactions and molecular transformations. This list of applications is far from complete and new ideas concerning the possible use of TiO_2 have been appearing regularly.

1.5. Zinc Oxide

1.5.1.Crystal structure

Zinc oxide normally occurs in the hexagonal wurtzite structure,[21] can be transformed to the cubic rocksalt (NaCl) structure by the application of high pressure. This cubic phase has been reported to be metastable at atmospheric pressure. ZnO has many attractive properties, such as the direct wide bandgap (3.37 eV), large exciton binding energy (60 meV at room temperature), good piezoelectric characteristics, chemical stability and biocompatibility. These properties suggest a host of possible practical applications, notably in the area of ultraviolet/blue emission devices.[22]

1.5.2. Synthesis methods

So far, nanocrystalline ZnO with different particle morphologies and sizes have been obtained by several preparation approaches including thermal decomposition, vapor chemical deposition, sol–gel method, wet chemical synthesis, mechanochemical, electrodeposition, gas-phase reaction, hydrothermal synthesis and so on.[1] Among other established synthesis methods, simple and cost effective routes to synthesize nanocrystalline ZnO by utilization of cheap, nontoxic and environmentally precursors are still the key issues. The commercial production of nano ZnO is currently achieved by the two mentioned main methods that represent ‘top-down’ and ‘bottom-up’ approaches. These are physical vapour synthesis (PVS) and mechanochemical processing (MCPTM).[1]

1.5.3. Applications

ZnO has interesting and wide applications in ceramics, catalysis,

rubber, cosmetics, varistors, ect. The size, morphology and charge of ZnO particles play an important role in these applications. Nanosize ZnO particles are efficient in killing many bacteria. Thin films or nanoscale coating of ZnO nanoparticles on suitable substrates is also important for its potential applications as substrates for functional coatings, printing, UV inks, e-print, optical communications (security papers), protection, barriers, portable energy, sensors, photocatalytic wallpaper with antibacterial activity etc.[23]

1.6. Nickel Oxide

1.6.1.Crystal structure

NiO (bunsenite) is an important semiconductor and an antiferromagnetic material with a cubic rock salt-like structure.[24] Nickel oxide (NiO) is an interesting material due to its useful electronic, magnetic and catalytic properties.

1.6.2. Synthesis methods

Many methods have been used to prepare NiO nanocrystals.[25] Single crystal cubic NiO nanorods were synthesised by using precursor thermal decomposition in NaCl flux at 1173 K. However, there are few reports on synthesis of nanowire NiO with a simple solution method. Usually, nanostructured NiO was obtained by direct decomposition of nanostructured precursor $Ni(OH)_2$ in presence of ethylenediamine as solvent and coordinating agent, that was successfully applied in the fabrication of nanosized materials.

1.6.3. Applications

NiO can be used as electrode materials in battery systems. Nonstoichiometric nickel oxide is a good P-type semiconductor owing to its defect structure and it is also a potential gas sensor for NO_2, NH_3, and

H_2. The recently observed electrochromic behavior makes its possible application in ‘‘smart windows’’ with variable light transmission characteristics and active optical fibers.[26] Nickel oxide is a very interesting material due to its complex band structure. Pure NiO is classified as a ‘Mott- Hubbard insulator’ with room temperature conductivity less than 10^{-13} ohm^{-1} cm^{-1} in which electrical conduction at room temperature is due to holes of intermediate mass.

1.7. Silica Gel

1.7.1.Crystal structure

Silica gel, an oxide of the element silicon, is an amorphous, highly porous, partially hydrated form of silica. The structure of silica gel, the matrix of the primary silica gel particle consists of a core of silicon atoms joined together with oxygen atoms by siloxane bonds (silicon-oxygen-silicon bonds). On the surface of each primary particle some residual, uncondensed hydroxyl groups from the original polymeric silicic acid remain. These residual hydroxyl groups confer upon silica gel its polar properties. These hydroxyl groups react with the silane reagents to form bonded phases. The silica surface is quite complex and contains three types of hydroxyl group (Fig. 1.3).[27] The first is isolated silanols, consisting of a single hydroxyl group attached to a silicon atom which has three siloxane bonds joining it to the gel matrix. The second is geminal silanols, formed by two hydroxyl groups attached to the same silicon atom which, in turn, is joined to the matrix by only two siloxane bonds. The third is vicinal silanols, that have a single hydroxyl group but are close enough to give hydrogen-bonding with another hydroxyl group on the surface.

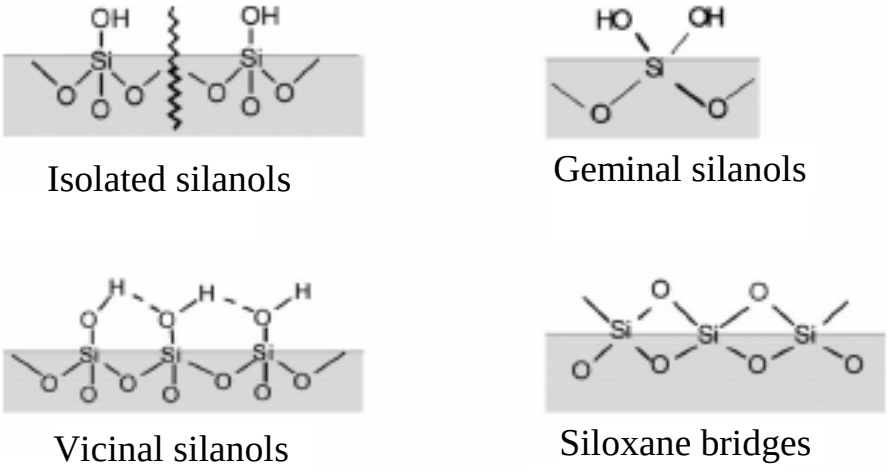

Fig. 1.3. Structures of the siloxane bridges and of the different silanol groups found on the surface of silica.

1.7.2. Synthesis methods

Irregular silica gel is prepared by releasing silicic acid from sodium silicate with hydrochloric acid. The silicic acid rapidly dimerises with elimination of water and then with further elimination of water forms trimers and in this way eventually polymerizes to a whietish translucent liquid. The polymer continues to grow forming polymer aggregate spheres a few Angstrom in diameter. When the spheres reach a particular size, the surface hydroxyl groups from different spheres condense forming a gel. The nanoparticle silica gel can often be prepared using assemblic materials during the preperation method.

1.7.3. Applications

Silica gel is non-toxic, non-flammable and chemically unreactive. Silica gel has high surface area which allows it to absorb water readily, making it useful as a desiccant (drying agent).[28] Silica gel is most commonly encountered in every day life as beads packed in a semi-permeable plastic. In this form, it is used as a desiccant to control local humidity in order to avoid spoilage of some goods. Because of poisonous

dopants and their very high absorption of moisture, it was used to protecting military equipment from moisture damage, as a fluid cracking catalyst for the production of high octane gasoline, and as a catalyst support for the manufacture of butadiene from ethanol, feedstock for the synthetic rubber. Silica gel is also used to dry the air in industrial compressed air systems, and in chromatography as a stationary phase. It is also applied to aluminum or plastic sheets for thin layer chromatography. Silica gel is also used as cat litter. It has been used widely in the industry and it possesses a moderate hydrophobicity. Silica gel has good light transmission and adsorption of contaminants. Recently, silica gel is used to support TiO_2 and nanocrystal-dispersed SiO_2 coatings have been reported.[29]

1.8. Silver

1.8.1. Crystal structure

Silver is a metallic element which used in many applications. Silver crystallize as face-centered cubic structure (FCC).

1.8.1. Synthesis methods

The most frequent preparation of silver nanoparticles is the reduction of silver salts by sodium borohydride or sodium citrate.[30] However, there are also some novel routes to obtain colloidal silver such as reduction of silver nitrate in ethylene glycol, in the presence of polyvinylpyrrolidone (PVP) as stabilizing agent. Silver nanoparticles prepared also via an amine adduct by the reaction of insoluble silver myristate with tertiary alkyl amine. It can be also prepared by reduction of silver nitrate with ascorbic acid in the presence of a polymeric steric stabilizer.[31]

1.8.1. Applications

Applications of fine metal particles to catalyst, electronic materials and sensors has been gradually increased. For example, fine silver particles of high purity were used as conductive paste and adhesive additives for electrodes and electric parts. Colloid of silver particle in nanometer size has been used as materials for conductive and transparent thin film. Bulk Ag has been long used for coatings many items including mirrors (for reflectance properties) and electrical contacts, as it is the most conductive of all metals. Silver has been widely used as an antimicrobial agent in applications such as wound dressings and as surface coatings for, e.g., catheters.[32]

1.9-Biological Activity

Microorganisms such as bacteria, algae and viruses adhere on the metal surfaces to form a biofilm within 3 days. The attached microorganisms excrete extracellular polymeric substances (EPS) which also contributes to the formation of biofilm. Biofilm formation creates serious problems of hygiene, odour and taste in cooling water as well as in drinking water systems. The attachment of biofilm on the walls of metal surfaces encourages pitting corrosion of mild steel, copper, etc.. Microbes should be killed in drinking water or should be removed in cooling water system to protect the materials against corrosion.[33] The formation of biofilm can be controlled by addition of biocides viz. sodium thiocyanate, bromine-based compound, ozone or chlorine in cooling water system. This treated water will be having toxic components, like chlorination of water leads to the formation of dangerous chlorinated hydrocarbons and ozonization treatment also encourages carcinogenesis. Therefore,

alternative technologies are required for water purification for their effective application. Since the biocides are toxic to human beings, cheaper, fool proof and ecofriendly technology is needed for cooling water system. Hence, it is the right time to identify the non-toxic and ecofriendly technology to control microbial attachment in cooling water system. A great deal of attention has been focused in recent years on the development of nanocrystalline semiconductor thin film of titanium dioxide (TiO_2) for drinking water treatment or cooling water industries as photocatalyst for its oxidative degradation of organic compounds as well as micro organisms. A microbial activity of UV/TiO_2 treatment has been assayed with respect to many bacteria and viruses. When illuminated with wavelength shorter than 385 nm, TiO_2 photocatalyst generates a strong oxidising power. Upon irradiation with a photon, an electron is excited to the conduction band leaving a hole (h^+) in the valance band. The activated electron reduces the adsorbed O_2 to produce $O_2^{\cdot -}$, while the hole oxidizes the adsorbed H_2O to produce a hydroxyl radical $OH^{\cdot}$.[34] Reactive oxygen species (ROS), produced in these reactions, are involved in a variety of oxidative effects. They interact with cellular membranes, inhibit enzyme activity, and destroy genetic supramolecules.

There is particular interest in nano-particulate Ag due to its ability to act as both an electron sink and as redox catalyst. The antimicrobial properties of silver were well known to the ancient Egyptians and Greeks, for example Hippocrates mentions the use of silver as a treatment for ulcers. Since silver has been widely used as an antimicrobial agent in applications[32] such as wound dressings and as surface coatings for, e.g., catheters. Silver has also been incorporated into bioglass. Silver ions (Ag^+) interact strongly with electron donors and the antimicrobial activity of Ag primarily involves interactions with sulphydryl groups in proteins. Silver

also reacts with other cellular components such as nucleic acids. Silver has been shown to inhibit energy production by inhibition of the respiratory chain of Escherichia coli (E. coli). Indirect toxicity may also arise from salt formation with silver ions that results in a chloride or anion limitation within the cell. Nanocrystalline silver also releases Ag^0 and has been shown to rapidly kill bacteria and fungi. Although Ag^+ is rapidly inactivated by interaction with organic matter, Ag^0 is much more stable.**(32)**

Microbial pollution and contamination by microorganisms have produced various problems in industry and other vital fields, such as degradation and infection. In order to solve these problems, new pasteurization and antibacterial techniques have been demanded and studied. The antibacterial activity of ceramic powders has attracted attention**(35)** as a new technique that can substitute for conventional methods using organic agents. Ceramic powders of zinc oxide (ZnO), calcium oxide (CaO) and magnesium oxide (MgO) were found to show marked antibacterial activity. The use of these ceramics has the following advantages: they contain mineral elements essential to humans and exhibit strong antibacterial activity in small amounts without the presence of light. It was found that ZnO exhibits antibacterial activity at pH values in the range from 7 to 8, and these values are suitable for use in water used for washing and drinking. Antibacterial activity of ZnO is considered to be due to generation of hydrogen peroxide (H_2O_2) from its surface. However, it is not yet clear what changes in antibacterial activity are expected due to the particle size of ZnO.

1-10. Literature Survey

Mesoporous anatase TiO_2 was prepared for photocatalysis from $TiOSO_4$ solution.[36] The samples were undoped or doped with chromium. The morphology of the TiO_2 particles exhibited strong dependency on the preparation conditions. The mesoporous samples showed good photo-activity upon degradation of acetaldehyde in the visible range (> 400 nm) and on degradation of methylene blue in aqueous solution in the UV range (366 nm). The catalyst activity demonstrated strong dependency on crystal size, on particle morphology and porosity, and on doping. The pore size of the samples increased upon heating.

Sheng et. al.[37] reported that a mesoporous TiO_2 with high photocatalytic activity was synthesized by assembling nanocrystalline particles using dodecylamine (DDA) as organic linkers. Low-angle XRD and TEM confirmed that the mesoporous TiO_2 had a wormhole-like structure. Nitrogen adsorption–desorption isotherm showed products retained mesoporosity with a narrow pore size distribution (2.8–4.0 nm) and high surface areas (104.4–346.0 m^2/g) to 673 K. TG-DTA analysis revealed that the surfactant had been removed partly in as-synthesized samples. The pH value affected the order of mesoporous structure. The ordered mesoporous structure would not retain at pH = 14. All calcined mesoporous TiO_2 showed high photocatalytic activities on photode-composition of cationic dye X-GL.

Yu et. al.[38] observed the formation of nanosized TiO_2 powder during chemical vapor condensation process. For this purpose, the powders were sampled at various positions in the furnace using a quartz collecting rod of which surface acts as the powder condensation site. It was discussed in terms of size effect on the phase stability that the fine anatase particle

transformed to the coarse rutile phase by growing in the high temperature region. Also the parabolic particle growth with the distance of reaction tube was explicated by computated residence time with solving temperature and gas velocity distribution.

Okuyamaa et. al.[39] synthesised Titanium oxide (titania) nano-particles (with a nominal size of about 10 nm) directly from three organic precursors: titanium tetraisopropoxide, and water-soluble titanium sources, by using a low-pressure spray pyrolysis method. Effects of temperature, solvent, concentration and precursor type have been investigated systematically. It was found that a higher temperature and a higher concentration were beneficial for the formation of nanoparticles. Addition of ethanol as a co-solvent improved breakup of droplets, and subsequently formation of nanoparticles. Water-soluble titanium sources showed great potentials for preparation of titania nanoparticles. The nominal size of nanoparticles calculated from electron microscopical images agreed well with that estimated from corresponding X-ray diffraction patterns, implying that nanoparticles were single crystals.

The effect of microstructural features on the electrical properties of TiO_2 (rutile) was studied using impedance spectroscopy in conjunction with X-ray diffraction and scanning electron microscopy.[40] It was found that the electrical resistivity increased significantly after the interconnected pores closed in the TiO_2 due to sintering. However, further decrease of porosity in the TiO_2 had little effect on its resistivity prior to the closure of pores. On the other hand, after the sintered specimens were annealed in vacuum, the resistivity of TiO_2 decreased considerably without apparent change of the microstructure in TiO_2. Moreover, the resistivity measured at room temperature, decreased after the interconnected pores closed due to sintering. These results suggest that the electrical conduction in TiO_2 after

sintering in air is mainly due to ionic conduction, while the conduction in the sintered TiO_2 after annealing in vacuum was mainly due to electronic conduction. The closer of the open pores in the TiO_2 reduced the surface ionic conduction but increased the electronic conduction route. Overall, the microstructural features of TiO_2 have characteristic effects on its electrical properties.

The electrical properties of low temperature (423 K) plasma deposited TiO_2 gate dielectrics on strained-Si are reported.[41] The interfacial and electrical properties of the deposited films have been characterized using a metal–insulator–semiconductor (MIS) capacitor structure. The charge trapping properties in TiO_2 gate dielectrics have been studied using constant current stressing. The leakage current has been found to be dominated by the Poole–Frenkel emission.

The modification of the surface chemistry of semiconducting nanoparticles is often required for optimising their performance.[42] For example, surface modifications of semiconductor-based sensors can be envisaged to tailor the device selectivity. However, surface chemical modifications should deteriorate neither the bulk characteristics nor the electrical properties of the material. This becomes critical for nanoparticles due to their high surface-to-bulk ratio. The surface modifications of titanium oxide nanoparticles by grafting hexamethyldisilazane (HMDS) are monitored in situ by Fourier transform infrared spectroscopy. The HMDS grafting decreases the density of the hydroxyl groups at the titanium oxide surface and therefore modifies the surface affinity to water molecules. The consequences of these surface modifications on the gas sensing properties of the nanomaterial are discussed. In particular, it is shown how moisture adsorption subsequently alters these new grafted chemical species, resulting in a decrease of the cross-sensitivity to

humidity. The variations of the infrared background absorption versus gas exposures are demonstrated to follow a dependence in agreement with the Drude–Zener theory, thus indicating that they are essentially due to the free carrier absorption.

Radio frequency (RF) plasma enhanced chemical vapor deposition of titanium oxide films for bactericidal applications is reported.[(34)]. The films were deposited on glass and cotton textile substrates. Optical properties, namely refractive index and extinction coefficient of the films deposited on glass were used as criteria for their quality. Bactericidal properties were studied using cultures of K12 strain of Escherichia coli and the ultraviolet light C (UV-C) irradiation. An effect of an RF power of the discharge on both the optical and the bactericidal properties of the films was investigated. The results showed a substantial enhancement of the bactericidal activity of UV irradiation for the surfaces modified with the presented process. A strong correlation between the bactericidal efficiency of the films and their refractive index has been reported.

Photocatalytic action of the commercial TiO_2 was the subject of study on the destruction of the microbes within the biofilms.[(33)] The TiO_2 powder was characterized by X-ray diffraction (XRD) for identifying its type and the particle. The biofilm was allowed to form over TiO_2 coatings over glass slides irradiated with polychromatic light for different time durations and distances. It indicates that a five-fold decrease in bacterial count due to the formation of H_2O_2 at TiO_2/biofilm interface. The formation of H_2O_2 at the TiO_2/biofilm interface is estimated and it does not destroy the entire bacterial population within the biofilm. Bacterial killing effect is supported by FT-IR analysis.

Simulated wastewaters that contain methylene blue (MB) were bleached in a photocatalytic aqueous TiO_2 dispersion illuminated by

concentrated sunlight using a parabolic round concentrator reactor.[43] The kinetic analysis was carried out well when the temporal concentration variation was a function of the concentrated light energy irradiated. The photocatalyzed N-demethylation of MB takes place concurrently with photocatalytic decomposition of MB by pseudo-first-order kinetics. The dependence of the photo-decomposition kinetics on the initial concentration of MB is consistent with the Langmuir–Hinshelwood model. Elimination of TOC (total organic carbon) also occurs by pseudo-first-order kinetics prior to full bleaching of the aqueous TiO_2 dispersion, after which the TOC level decreases only slightly. Also, compared with the open to air, the photodegradation of MB is not influenced by molecular oxygen bubbling continuously through the reactant suspensions during illumination. TiO_2 loadings and flow rates markedly affect the degradation of MB. Under concentrated sunlight, the relative photonic efficiency of MB photodegradation is 49 % (relative to phenol). The efficiency for the degradation of MB is independent of photoreactor geometry (cylindrical bottle reactor versus round-bottomed flask), of light sources (solar light concentrator versus a Hg lamp) and of the operating mode used (flow versus batch operation).

Photocatalytic degradation of methylene blue (MB) in aqueous solution was investigated using TiO_2 immobilized on activated carbon fibers (ACFs).[44]. Through measurement of chemical oxygen demand in the solution and the concentration of ammonium generated during degradation of MB, it was confirmed that MB molecules are mineralized instead of adsorbed by ACFs.

The photocatalytic degradation of five various dyes has been investigated in TiO_2/UV aqueous suspensions.[45] It was attempted to determine the feasibility of such a degradation by varying the chemical

structures, either anthraquinonic (Alizarin S (AS)), or azoic (Crocein Orange G (OG), Methyl Red (MR), Congo Red (CR)) or heteropolyaromatic (Methylene Blue (MB)). For azo-dye (OG, MR, CR) degradation, the complete mass balance in nitrogen indicated that the central –N=N– azo-group was converted in gaseous dinitrogen, which is the ideal issue for the elimination of nitrogen-containing pollutants, not only for environmental photocatalysis but also for any physicochemical method. The aromatic rings were submitted to successive attacks by photogenerated $OH^{\bullet}$ radicals leading to hydroxylated metabolites before the ring opening and the final evolution of CO_2 induced by repeated subsequent "photo-Kolbe" reactions with carboxylic intermediates. These results suggest that TiO_2/UV photocatalysis may be envisaged as amethod for treatment of diluted colored waste waters not only for decolorization, but also for detoxification, in particular in textile industries in semi-arid countries.

The TiO_2/UV photocatalytic degradation of methylene blue (MB) has been investigated in aqueous heterogeneous suspensions.[46] In addition to a prompt removal of the color, TiO_2/UV-based photocatalysis was simultaneously able to oxidize the dye, with an almost complete mineralization of carbon and of nitrogen and sulfur heteroatoms into CO_2, NH_4^+, NO_3^- and SO_4^{2-}, respectively. These results suggest that TiO_2/UV photocatalysis may be envisaged as a method for treatment of diluted waste waters in textile industries.

Titanium dioxide nano-crystalline thin films on glass, polycarbonate, polymethyl methacrylate, and aluminum were prepared via a sol–gel process using different alkoxide precursors.[47] All specimens exhibited nano-sized (<10 nm) crystals of the anatase phase with a very tiny amount of brookite phase. The surface morphology of the thin film was influenced

by the nature of the substrate. As the thickness of the thin film increased, the effect of the substrate diminished in terms of photocatalytic decomposition of methylene blue solution. Surface morphology and thereby photocatalytic reactivity of the TiO_2 thin films can be tailored by proper heat treatment. The maximum photocatalytic decomposition of methylene blue solution was achieved with a heat treatment at 673 K, which was ascribed to the enlarged surface area upon morphological change of the surface.

Photocatalytic degradation of methylene blue (MB) in TiO_2 aqueous suspensions using microwave (MW) powered electrodeless discharge lamps (EDLs) was studied.[48] The process was promising in treating MB polluted water.

Aqueous solutions of Safranin-T, a hazardous textile dye, are photodegraded under ultraviolet light using TiO_2 as catalyst.[49] The process has been carried out at different pHs, amounts of catalyst, concentrations of the dye, and effects of the electron acceptor H_2O_2. Measuring chemical oxygen demand also monitors the toxicity of the degraded dye solution and a significant decrease is observed, which implies that the photodegradation through TiO_2 is a safer technique.

The 8–10 nm pure anatase phase titania with 156 m^2/g BET surface area was prepared by solution combustion method.[50] This catalyst was used for the photocatalytic degradation of various dyes such as heteropolyaromatic dye (Methylene blue), anthraquinonic dye (Alizarin S), and azoic dyes (Methyl red, Congo red, and Orange G). Substitution of TiO_2 with transition metal had a detrimental effect on the photocatalytic activity. However, this inhibition effect was not observed with Pt impregnated TiO_2. This was attributed to the metals being in ionic state in metal substituted TiO_2 synthesized by combustion method, and zero state

of metal in impregnated catalysts as evidenced by XPS study. The degradation of dyes was also investigated in solar exposure. The photoactivity of the combustion synthesized titania was higher than commercial TiO_2 (Degussa P-25) for both UV and solar exposure. The experimental data followed Langmuir–Hinshelwood (L–H) rate form and the kinetic parameters were obtained.

Andronic and Duta[(51)] investigate the influence of the TiO_2 specific surface (powder, film) on the photocatalytic degradation of methyl orange. Porous TiO_2 films were deposited on transparent conducting oxide substrates by spray pyrolysis deposition. The XRD spectra of nanoporous TiO_2 films revealed an anatase, crystalline structure that is known as the most suitable structure in photocatalysis. The average thickness of the films was 260 nm and the measured band gap is 3.44 eV. The influence of the operational parameters (dye concentration, contact time) on the degradation rate of the dye on TiO_2 was examined.

Baran et. al.[(52)] examined the correlation between the absorbance of various cationic and anionic dye solutions exposed to UV radiation and their photocatalytic degradation in solution. The dye solutions were illuminated with UV radiation in the presence of a TiO_2 aqueous suspension. Photodegradation rate constant and adsorption efficiency of dyes were determined using spectrophotometric methods. Only cationic dyes can be adsorbed on the surface of the photocatalyst; simultaneously, their photocatalytic degradation is faster than the degradation of anionic dyes. The change of the nature of the dye particle from inert to cationic causes intensification of its adsorption and acceleration of photodegradation. There is a linear correlation between the absorbance of the illuminated dye solution and the photodegradation rate constant.

Madras et. al.[(53)] studied The solar photocatalytic degradation of

various dyes such as methylene blue (MB), remazol brill blue R (RBBR) and orange G (OG) over combustion synthesized nano TiO_2 and the activity was compared with that of commercial Degussa P_{25} TiO_2 under similar conditions. The effect of catalyst loading, initial concentrations of the dyes and the deactivation studies of the catalysts were also investigated. The initial degradation rates with combustion synthesized nano TiO_2 was 20 times higher for RBBR, 4 times higher for MB and 1.6 times higher for OG, compared to Degussa P_{25} TiO_2. The enhanced photocatalytic activity of combustion synthesized catalyst is attributed to the crystallinity, nano-size, large amount of surface hydroxyl species and reduced band-gap.

Messina and Schulz[(54)] studied the adsorption of two basic dyes, methylene blue (MB) and rhodamine B (RhB), from aqueous solution onto mesoporous silica–titania materials. The effect of dye structure, adsorbent particle size, TiO_2 presence and temperature on adsorption was investigated. Adsorption data obtained at different solution temperatures (298, 308, and 318 K) revealed an irreversible adsorption that decreased with the increment of Temperature. The presence of TiO_2 augmented the adsorption capacity *(*q_e*)*. This would be due to possible degradation of the dye molecule in contact with the TiO_2 particles in the adsorbent interior. The adsorption enthalpy was relatively high, indicating that interaction between the sorbent and the adsorbate molecules was not only physical but chemical. The obtained parameters and correlation coefficients showed that the adsorption of the two reactive dyes (MB and RhB) on the adsorbent systems at the three work temperatures was best predicted by the Langmuir isotherm, but not in all cases. The kinetic adsorption data were processed by the application of two simplified kinetic models, first and second order, to investigate the adsorption mechanism. It was found that

the adsorption kinetics of methylene blue and rhodamine B onto the mesoporous silica–titania materials surface under different operating conditions was best described by the first-order model.

The preparation, activity and characterization of TiO_2 clusters on several of textiles are presented having a self-cleaning effect under daylight irradiation.[55] The textile pretreatment was carried out by RF-plasma, MW-plasma or vacuum-UV irradiation. The textile upper layers are modified in such a way that negatively charged TiO_2 chelating groups such as carboxylic groups are introduced by the pretreatment methods used. The pretreatments used in this study were applied in dry conditions in the absence of solvents. Also, the times employed for the cotton surface modification were short and involved reduced energy requirements. The quantitative results obtained during the discoloring of spots of wine, coffee, makeup and grease indicate that the photoactivity observed on the TiO_2 modified textiles upper layers strongly depends on the nature of the TiO_2 used and on the procedure used to apply the TiO_2 on the textile. When light is harvested directly by the TiO_2, like in the case of grease stains an increased CO_2 evolution was observed with respect to wine and coffee stains under similar experimental conditions on the same TiO_2 loaded textile. Also, chemical spacers able to graft TiO_2 on suitable functional groups of the textile and through a second link bond to the TiO_2 clusters have been studied with promising results in photoactivated light induced discoloration processes.

Nanostructured titanium dioxide materials were synthesized hydrothermally ($TiCl_4$, 353 K, 5 days) via assembling through cationic surfactants in particular cetyltrimethylammonium bromide (CTAB) and cetylpyridinum bromide (CPB).[56] The results revealed that the crystallites size of all materials lie in the range of 10.1-18.2 nm and organized in a

morphological structure that change from nano-sized spheres to cotton fibrils shape. Surfaces thereon exposed were found to assume high specific areas (240-418 m^2 g^{-1}) and micro-mesoporous surfaces with pore size in the range 23.2-43.7 Å. Rutile phase was only produced for all TiO_2 materials assembled by cationic surfactants following heating up to 623 K. The transformation of rutile to anatase TiO_2 was coincided with the developed interaction between vanadia and titania assembled by CPB template. The V in the resulting vanado-titanate was entirely incorporated in TiO_2 structure. The assynthesized phases of either rutile or anatase were maintained after calcining at 973 K exhibiting a significant thermal stability. Pyridine adsorption at room temperature indicated the involvement of acid-base site pair on all TiO_2 assembled by cationic templates where that prepared by conventional method only exposed Lewis and Brönsted acid sites with a higher tendency to the latter comparatively.

Nanostructured titanium dioxide and vanadium oxide supported over titanium dioxide was synthesized using a template synthesis route method under hydrothermal conditions (at 353 K for 5 days) via sodium dodecyl sulfate surfactant.[(57)] The influence of pH (2.0–12 9.0) and thermal treatment (623 and 773 K) on the structural, surface acidity and textural properties of TiO_2 and V_2O_5/TiO_2 materials was investigated. The synthesized TiO_2 and V_2O_5/TiO_2 showed high mesoporosities with different pore sizes ranging from 24.6 to 40.6A ° and exhibited nano-sized crystals varying from 7.5 to 15.1 nm. All templated samples exhibited very high surface areas; commencing from 263 to 465 m^2/g, as well as pore volume up to 0.73 cm^3/g. The synthesized samples exhibited a pure anatase crystalline phase for TiO_2 in the pH range 4.8–9, in which substantial amounts of mesopores were developed where that prepared at pH = 2.0 showed the formation of only rutile phase with higher affinity to

micropores. Surface acid strength was greater for highly dispersed V containing TiO_2 due to a strong interaction of the VO_x species with support centers that act as electron attractor centers creating Lewis acid sites. It was found that pH has a paramount effect influencing both the nature of pores and the type of TiO_2 formed. The photocatalytic reduction of Hg^{2+} in water by UV irradiation was chosen to evaluate the activities of the synthesized materials.

It was shown[(58)] that a solar driven, self-cleaning coating was deposited onto organic fluorocarbon paint using a hybrid system. The system utilizes the corona treatment technique, the inert sol–gel coating and the anatase TiO_2 layer. With the corona treatment, an organic surface was activated to allow a uniform TiO_2 sol–gel coating. This sol–gel layer has two functions: firstly, it acts as binder to adhere the nanosize TiO_2 particles; secondly, it acts as barrier to prevent substrate-damage from the photocatalytic reaction. Using this approach, a strong and crack-free TiO_2 sol–gel coating was obtained. The very fresh TiO_2 sol–gel coating shows almost zero water contact angle even without exposure to sunlight, and this super-hydrophilic property is retained under sunlight irradiation. With such photocatalytic and hydrophilic characteristics, dirt residues on the surface were either readily oxidized or simply washed away by rain.

Nguyen et. al.[(59)] demonstrated the effect of pre-thermal treatment of TiO_2 nano-particles on the performances of dye-sensitized solar cells (DSCs) by using high specific surface area and anatase only TiO_2 nano-particles (ca. 340 m^2/g, Sachtleben Chemie GmgH, represented as HK). TiO_2 particles and thin films were characterized with X-ray diffraction, FT-IR, UV–Vis diffuse reflectance spectroscopy and FE-SEM. The photoelectrochemical properties of the thin films and the performances of DSCs were measured by photocurrent densities, AC impedance spectra and

photocurrent–voltage curves. Before coating the raw TiO_2 of HK (HK-raw) on transparent conducting oxide (TCO) glass for DSC fabrication, pre-thermal treatment of HK raw by calcining at 723 K (HK-723) was an essential step to achieve the optimum properties in terms of morphological feature, crystallinity, specific surface area and photocurrent density. HK-450 film showed the high adsorption of dye, high photocurrent density and low interface resistance between TiO_2 and TCO glass, $RTiO_2$/TCO and TiO_2 and redox electrolyte, RCT, resulting in the superior photovoltaic performance on the DSC fabricated with HK-723 and Eosin Y (or ruthenium 535 bis-TBA). Accordingly, the optimization between the morphological feature, specific surface area and photocurrent density of TiO_2 substrate is promising to accomplish the improved overall conversion efficiency of DSC.

Mechanochemical processing involves the mechanical activation of solid-state displacement reactions at low temperatures in a ball mill.**(60)** Milling of precursor powders leads to the formation of a nanoscale composite structure of the starting materials which react during milling or subsequent heat treatment to form separated nanocrystals of the desired phase within a solid matrix. Such mechanochemically formed nanocomposite particles can be further processed into dispersed nano powders simply by selective removal of the matrix phase. The synthesis of ZnO nanoparticles via the mechanochemical reaction $ZnCl_2 + Na_2CO_3 \rightarrow 3ZnCO_3 + 2NaCl$ has been studied.**(61)** A solid-state displacement reaction between $ZnCl_2$ and Na_2CO_3 was induced by mechanochemical processing in a steady state manner, forming $ZnCO_3$ in a NaCl matrix. Heat treatment of the as-milled powders at 673 K led to the thermal decomposition of $ZnCO_3$, resulting in ZnO nanoparticles embedded in the NaCl matrix. The mean particle size was ; 27 nm. Since the mechanochemically formed

$ZnCO_3$ nanoparticles were isolated in the NaCl matrix, sintering of the ZnO powder did not occur during heat treatment. The particles had nearly uniform equiaxed shapes, and a narrow size distribution. Mechanochemical processing is particularly suitable for a large scale production of ZnO.

A novel sisal-like ZnO nanostructures have been synthesized through a simple chemical vapor deposition (CVD) approach.**(61)** The nanoleaves of the ZnO nanosisals are single-crystalline wurtzite structures and preferentially oriented in the <001> direction.

ZnO nanorods had been successfully prepared by annealing the precursors, which are produced by the chemical precipitation method.**(62)** The annealing temperature is found to be a key parameter for the preparation of ZnO nanorods. The largest ratio of the length to diameter for nanorods has been obtained at the annealing temperature of 673 K.

Synthesis of ZnO nanorods have been prepared by thermal decomposition of the precursor of ZnC_2O_4 obtained via chemical reaction between $Zn(CH_3COO)_2.2H_2O$ in the presence of surfactant nonyl phenyl ether(9)/(5) and NaCl flux.**(63)** The nanorods were characterized by techniques such as XRD, TEM, XPS and Raman spectra. The results showed that the as-prepared nanorods are composed of ZnO with diameter of 10-60 nm, and lengths ranging from 1 to 3 μm. The mechanism of formation of ZnO nanorods was also discussed.

An aqueous solution of monodispersed ZnO nanorods was prepared with $ZnCl_2$ as raw material and PVP as surfactant by a simple chemical reduction.**(64)** The influence of experimental conditions, such as reaction time, quantity of PVP and concentration of Zn^{2+}, etc. on the quality of the nanorods were discussed. Through altering Zn^{2+}/PVP weight ratio, the size of ZnO could be controlled.

ZnO nanoparticles with spherical morphology and narrow size

distribution were obtained by calcination of $Zn(OH)_2$ nanoparticles,[65] which were prepared in a polyethylene glycol mono-4-nonylphenyl ether (NP-5)/cyclohexane reverse micellar system and incorporated into polyurea (PUA) via an in situ polymerization of hexamethylene diisocyanate (HDI).

The ZnO particles were prepared by implementing the precipitation transformation method from $Zn_5(CO_3)_2(OH)_6$ in an aqueous solution at a low temperature (room temperature to 343 K).[66] The phase transformation process was detected by using a pH-meter and an X-ray diffraction (XRD).With an increase of temperature and concentration and quantity of NaOH solution, the ZnO phase became easier to form, otherwise, the ε-$Zn(OH)_2$ phase would need to be formed. The morphology of ZnO particles and its formation mechanism were investigated. Through controlling the reaction conditions and the post-treatment, the ZnO nanoparticles can be obtained.

Fan et. al.[67] reported the growth mechanism and structural properties of micrometer sized ZnO cages which were synthesized directly from Zn vapor deposition and oxidation. The ZnO microcages exhibit a hexagonal or spherical shape with partly or completely open surfaces and hollow interiors. The growth process of the microcages includes the deposition of Zn polyhedral particles, top face breaking of the Zn particles, Zn sublimation and subsequent reaction to ZnO. The room-temperature photoluminescence spectrum indicates a large quantity of oxygen-vacancy related defects within the wall of the ZnO cages.

Maensiri et. al.[68] reported the synthesis and characterization of nanocrystalline ZnO powders by a simple method using zinc acetate dihydrate and polyvinyl pyrrolidone (PVP) as a chelating agent. The precursor was calcined at 873 K for 1 h to obtain nanocrystalline ZnO

powders. The morphology and crystalline size of the calcined powders characterized by SEM and TEM revealed that the powders consisted of the mixture of nanoparticles with particle sizes of 50–100 nm and nanorods with diameters of 100–200 nm and 200–500 nm in length. The XRD and FT–IR results indicated that the synthesized ZnO powders had the pure wurtzite structure .

Wurtzite-type ZnO particles were directly prepared in agar gel containing zinc sulfate by diffusion of hydroxyl ions (OH^-).[(69)] A banded structure consisting of characteristically shaped particles, such as star-like, ellipsoidal, and round grains, was obtained through periodic precipitation along the direction of the OH^- diffusion. The individual particles were composed of nanoscale ZnO crystallites elongated in the c-axis. The star-like and ellipsoidal ZnO aggregates were produced through a dissolution–precipitation process from previously precipitated thin plates of $ZnSO_4$ - $3Zn(OH)_2$. The gel media provided a diffusion field of the precursors resulting in the formation of various kinds of characteristic shapes consisting of nanoscale ZnO particles.

Vertically aligned ZnO nanowires were synthesized on the pC silicon chip by modifying the CVD process with a vapor trapping design.[(70)] Scanning electron microscopy was used to investigate the morphology of as-obtained nanowires. X-ray diffraction showed that the obtained nanowires were ZnO crystalline. The rectifying characteristics of the p–n heterojunction composed of ZnO nanowires and a p^+ silicon chip were observed. The positive turn-on voltage was 0.5 V and the reverse saturation current was 0.01 mA. These vertically aligned ZnO nanowires showed a low field emission threshold of 4 V/mm at a current density of 0.1 mA/cm^2.

The antibacterial behaviour of suspensions of zinc oxide

nanoparticles (ZnO nanofluids) against E. Coli has been investigated.[71] ZnO nanoparticles from two sources are used to formulate nanofluids. The effects of particle size, concentration and the use of dispersants on the antibacterial behaviour are examined. The results show that the ZnO nanofluids have bacteriostatic activity against E. coli. The antibacterial activity increases with increasing nanoparticle concentration and increases with decreasing particle size. Particle concentration is observed to be more important than particle size under the conditions of this work. The results also show that the use of two types of dispersants (Polyethylene Glycol (PEG) and Polyvinylpyrolidone (PVP)) does not affect much the antibacterial activity of ZnO nanofluids but enhances the stability of the suspensions. SEM analyses of the bacteria before and after treatment with ZnO nanofluids show that the presence of ZnO nanoparticles damages the membrane wall of the bacteria. Electrochemical measurements using a model DOPC monolayer suggest some direct interaction between ZnO nanoparticles and the bacteria membrane at high ZnO concentrations.

Coating of ZnO nanoparticles on paper surface has potential technological applications.[23] With this motivation, a simple approach of ultrasound assisted coating of paper with ZnO nanoparticles (20 nm) without the aid of binder is reported for the first time in this work. The ultrasound assisted coating approach concurs with ‘‘green’’ chemistry as it is simple and environmentally friendly. Scanning electron microscope is used to characterize the surface morphology showing ZnO nanoparticles bound to cellulose fibers. The ZnO nanoparticles coated paper is found to possess antibacterial activity against Escherichia coli 11634.

Zinc oxide powders were heated in different atmospheres at 1073 K and 1673 K, of which the characterization and the antibacterial activity were studied[72] by X-ray diffractometry and the measurement of the

change in electrical conductivity with bacterial growth. The diffraction peaks corresponding to zinc oxide with hexagonal type structure were detected in all samples, which shifted in low-angle side with the increase in the oxidizability of atmosphere during heat-treatment. From the results of calculating lattice constants, a_0 and c_0, it was found that the value of c_0 in hexagonal structure increased with the increase in the oxidizability of atmosphere. On the samples heated at 1673 K, the changes of the $c_o$value were less than those at 1073 K. However, no change of the a_o value showed, irrespective of atmosphere and temperature. Hydrogen peroxide that contributes to the occurrence of antibacterial activity was found to generate from all samples, and the generation amount increased with the increase of c_o value; incidently the amount in the samples heated at 1673 K was less than that at 1073 K. The antibacterial activity of zinc oxide increased with the increase of c_o value; that is, it was found that the value of c_o in crystal structure affected the antibacterial activity of zinc oxide.

The influence of particle size on the antibacterial activity of ZnO powders was investigated[(73)] using powders with different particle sizes ranging from 0.1 to 0.8 μm. By measuring the change in electrical conductivity with bacterial growth, it was found that the antibacterial activity of ZnO increased with decreasing particle size and increasing powder concentration. The changes of antibacterial action for Staphylococcus aureus were similar to those for Escherichia coli. However, the influence of particle size for Staphylococcus aureus was less than that for Escherichia coli.

Comparison of ZnO nanoparticles and its nano-crystalline particles on the photocatalytic degradation of methylene blue was investigated.[(74)] ZnO nanoparticles and its nano-crystalline particles were synthesized from sprayed droplets of an aqueous zinc nitrate solution by flame spray

pyrolysis and spray pyrolysis assisted with an electrical furnace, respectively. ZnO nanoparticles of 20 nm in average diameter and ZnO nano-crystalline particles of 20 nm in the grain size were prepared to compare the photocatalytic activity. The photocatalytic activity of those ZnO particles was evaluated by measuring the degradation of methylene blue in water under the illumination of ultraviolet rays. Effect of the particle morphology, initial concentration of methylene blue, and photocatalyst loading on the degradation of the methylene blue was investigated under the illumination of ultraviolet rays. The photocatalytic degradation capacity of the ZnO nanoparticles was higher than that of the ZnO nano-crystalline particles. The efficiency of photocatalytic degrade-ation of methylene blue increased with increase in photocatalyst loading and decrease in initial concentration regardless of particle morphology.

Zhou et. al.[25] were successfully developed for the synthesis of nickel hydroxide (theophrastite) nanoplatelets by a novel room-temperature coordination–precipitation technique. This method has great potential for large-scale industrial production owing to facile size-controlled and low-cost. This platelet-like nickel hydroxide precursor can readily be converted to nickel oxide (bunsenite) nanoplatelets after the calcination at 673 K. The thickness of β-$Ni(OH)_2$ nanoplatelets can be controlled by changing concentration of precipitant NaOH in the presence of ethylenediamine which play a crucial role in controlling phase composition of resulting precipitate.

Fu et. al.[24] prepared urchinlike NiO nanostructures by thermal decomposition of the precursor obtained via a hydrothermal process using urea as a hydrolysis-controlling agent and polyethylene glycol (PEG) as a surfactant. Structure characterizations indicated urchinlike nanostructures for the nickel oxide samples with high purity. Electrochemical properties

of urchinlike NiO were examined by cyclic voltammetry and galvanostatic charge–discharge measurements. The results showed that NiO calcined at 573 K had a higher specific capacitance and better capacitive behavior than NiO calcined at 773 K.

The synthesis of size-homogeneous and well-dispersed NiO nanoparticles of about 30 nm has been achieved.[(75)] In this method, the reaction temperature is 673 K. The mixture of nickel acetate and polyvinylpyrrolidone (PVP) is used as precursor. The NiO nanoparticles are composed of smaller nanoparticles.

Nickel oxide (NiO) nanowire was synthesized by a simple aqueous solution method with urea as a precipitant.[(76)] The structure, morphology and properties of the products were examined by X-ray diffraction (XRD), transmission electron microscopy (TEM), infrared absorption spectra (IR), and UV–visible absorption spectra. The results of the electrical and optical measurements made on these nanowire are discussed. The TEM images show the calcination product is NiO polycrystalline nanowire with diameters 5 – 15 nm. Thermal stability of this nanowire was studied by calcining the precursor at different temperatures and the breakdown of the precursor nanowire was observed after being calcined at 873 K for 2 h.

The synthesis of well-dispersed composite Ni/NiO nanoparticles of controlled size has been achieved[(77)] in organic solution in the presence of polyvinylpyrrolidone, using biscycloocta-1,5-diene nickel as a precursor, upon controlling the water and dioxygen content of the reacting medium. The oxidation of these particles into NiO nanoparticles can be achieved in mild conditions and preserves their dispersion in the polymer matrix.

DC conductivity of consolidated nanoparticles of NiO, having different average particle sizes (2.5 nm - 17 nm) was measured in the temperature range 313 K to 423 K.[(78)] The conductivity of NiO

nanoparticles are found to be enhanced by six to eight orders of magnitude over that of NiO single crystals. This large enhancement in conductivity is attributed to the high density of Ni^{+2} vacancy in the nanoparticles. Calculation of activation energy leads to the conclusion that the most prominent conductivity mechanism over the temperature range of observation is the large polaron conduction associated with holes in the 2p band of O^{2-}. The decrease in activation energy for the samples in comparison with that of the bulk material is explained on the basis of the enormously defective nature of nanoparticles. In the last part of the discussion, the effect of interfacial region on the electrical conductivity of the samples is analyzed, by taking into account the contributions due to grain boundaries and triple junctions. A semi-quantitative explanation for the observed variation of conductivity with particle size is presented on the basis of the assumption that the role of the triple junctions is to reduce the conductivity. The importance of triple junctions in determining the transport properties of nanoparticles is emphasized.

The attack of sand with a solution of sodium hydroxide allows to synthesize a soluble metasilicate.**(79)** Sodium ions were substituted by ammonium ions in order to synthesize pure silica gel. The obtained silica aerogels were amorphous. The variation of specific area and porous volume with silica concentration in the sol, with the pH of destabilization and the nature of destabilization acid were studied. The obtained aerogels were grafted by different organic molecules and characterized by high resolution solid state NMR.

Silica gels with trimethylsilyl and long-chain alkyl (C_6–C_{18}) groups have been synthesized.**(80)** It has been established that adsorption of water on silica gels modified with trimethylsilyl groups decreases substantially and varies as a function of the modifier and the synthesis method chosen.

The most hydrophobic surface (contact angle Θ =136°) is characteristic of silica modified with trimethyliodosilane vapor at 25°C. It has been shown that the lowest affinity for water (Θ=110–130°) is characteristic of silica gels modified with hydrocarbon radicals, i.e. of silica gels whose residual silanol groups were end-capped using vapor-phase modification with hexamethyldisilazane or trimethyliodosilane. The results presented account for the differences in hydrophobic properties of surfaces of silica gels modified with trimethylsilyl and long-chain alkyl groups.

The adsorption behaviour of various organic adsorbates on silica surface is reviewed.[81] Most of the structural information on silica is obtained from IR spectral data and from the characteristics of water present at the silica surface. Silica surface is generally embedded with hydroxy groups and ethereal linkages, and hence considered to have a negative charged surface prone to adsorption of electron deficient species. Adsorption isotherms of the adsorbates delineate the nature of binding of the adsorbate with silica. Aromatic compounds are found to involve the pi-cloud in hydrogen bonding with silanol OH group during adsorption. Cationic and nonionic surfactants adsorb on silica surface involving hydrogen bonding. Sometimes, a polar part of the surfactants also contributes to the adsorption process. Styryl pyridinium dyes are found to anchor on silica surface in flat-on position. On modification of the silica by treating with alkali, the adsorption behaviour of cationic surfactant or polyethylene glycol changes due to change in the characteristics of silica or modified silica surface. In case of PEG-modified silica, adsolubilization of the adsorbate is observed. By using a modified adsorption equation, hemimicellization is proposed for these dyes. Adsorptions of some natural macromolecules like proteins and nucleic acids are investigated to study the hydrophobic and hydrophilic binding sites of silica. Artificial

macromolecules like synthetic polymers are found to be adsorbed on silica surface due to the interaction of the multifunctional groups of the polymers with silanols. Preferential adsorption of polar adsorbates is observed in case of adsorbate mixtures. When surfactant mixtures are considered to study competitive adsorption on silica surface, critical micelle concentration of individual surfactant also contributes to the adsorption isotherm. The structural study of adsorbed surface and the thermodynamics of adsorption are given some importance in this review.

The potential eco-toxicity of nanosized titanium dioxide (TiO_2), silicon dioxide (SiO_2), and zinc oxide (ZnO) water suspensions was investigated[82] using Gram-positive Bacillus subtilis and Gram-negative Escherichia coli as test organisms. These three photosensitive nanomaterials were harmful to varying degrees, with antibacterial activity increasing with particle concentration. Antibacterial activity generally increased from SiO_2 to TiO_2 to ZnO, and B. subtilis was most susceptible to their effects. Advertised nanoparticle size did not correspond to true particle size. Apparently, aggregation produced similarly sized particles that had similar antibacterial activity at a given concentration. The presence of light was a significant factor under most conditions tested, presumably due to its role in promoting generation of reactive oxygen species (ROS). However, bacterial growth inhibition was also observed under dark conditions, indicating that undetermined mechanisms additional to photocatalytic ROS production were responsible for toxicity. These results highlight the need for caution during the use and disposal of such manufactured nanomaterials to prevent unintended environmental impacts, as well as the importance of further research on the mechanisms and factors that increase toxicity to enhance risk management

Silver colloid of nanometer was prepared in liquid phase by a

reduction method.[83] $AgNO_3$, $FeSO_4.7H_2O$ and $Na_3C_6H_5O_7.2H_2O$ were used as silver precursor, reducing agent and dispersing agent, respectiviely. As precursor concentration was decreased or the concentration of dispersing agent was increased, the prepared particle size was decreased from 180 nm to 20 nm. The particle size seemed to be decreased with the increase of stirring rate, but it was confirmed by TEM that the size of primary particle remained the same. This indicates that the uniformity of precursor concentration in the reactor affects the particle size and the stirring rate should be kept higher than the critical value to prevent the agglomeration of particles.

Dispertions of colloidal silver have been prepared by the reduction of silver nitrate,[84] with different reductants in the presence of various stablising agents. Aging these dispersions at room temperature for 2 h yielded particles with average sizes ranging from 1 nm up to 6 μm .The hexagonal phase hindered the growth and aggregation of particles. At the initial stage of the reaction, silver particles prepared in the hexagonal phase exhibited a size of 1-7 nm. As reaction proceed, particles grew up to about 30 nm. It was found that the reaction temperature was an important factor for the rate of particle formation.

Silver compounds have been exploited for their medicinal properties for centuries.[85] At present, silver is reemerging as a viable treatment option for infections encountered in burns, open wounds, and chronic ulcers. The gold standard in topical burn treatment is silver sulfadiazine (Ag-SD), a useful antibacterial agent for burn wound treatment. Recent findings, however, indicate that the compound delays the wound-healing process and that silver may have serious cytotoxic activity on various host cells. The present review aims at examining all available evidence about effects, often contradictory, of silver on wound infection control and on

wound healing trying to determine the practical therapeutic balance between antimicrobial activity and cellular toxicity. The ultimate goal remains the choice of a product with a superior profile of infection control over host cell cytotoxicity.

A range of morphologically nanoparticulate materials including Ag, NiO, TiO_2, multiwall carbon nanotubes, and chrysotile asbestos have been characterized[(86)] by transmission electron microscopy. All but the TiO_2 (anatase and rutile) were observed to exhibit some cytotoxicity at concentrations of 5 mg/ml for a murine macrophage cell line as a respiratory response model. Silver exhibits interesting systemic differences for animal and human toxicity, especially in light of its nanoparticulate materials, and should be avoided even if there is no detectable in vitro cytotoxic response, as a prudent approach to their technological applications.

The antibacterial properties of differently shaped silver nanoparticles were investigated against the gram-negative bacterium *Escherichia coli*, both in liquid systems and on agar plates.[(87)] Energy-filtering transmission electron microscopy images revealed considerable changes in the cell membranes upon treatment, resulting in cell death. Truncated triangular silver nanoplates with a (111) lattice plane as the basal plane displayed the strongest biocidal action, compared with spherical and rod-shaped nanoparticles and with Ag^+ (in the form of $AgNO_3$). It is proposed that nanoscale size and the presence of a (111) plane combine to promote this biocidal property. To our knowledge, this is the first comparative study on the bactericidal properties of silver nanoparticles of different shapes, and our results demonstrate that silver nanoparticles undergo a shape-dependent interaction with the gram-negative organism E. coli.

1.11. Aim of the Work

The objective of this work aims to study the effect of particle size in the range of nanometer on the physical and biological properties of Ag and some metal and non-metal oxides. The applications of these nanomaterials are parts of our targets. The program of this study includes:

(1) Literature review upon the problem under investigation.

(2) Selecting the proper methods to prepare the particle of investigated materials in the range of nano.

(3) Characterization for the prepared materials using different techniques such as thermal analysis (DTA, TG), FT-IR, X-ray diffraction (XRD), scanning electron microscope (SEM), transsimation electron microscope (TEM).

(4) Study the surface properties of the prepared materials such as surface area, adsorption capacity and surface acidity.

(5) Study electrical properties for some of prepared nanomaterials under different temperatures and frequencies such as electrical conductivity (σ) using dc- and ac-curent, dielectric constant (ε`), dielectric loss (ε``) and impedance (Z).

(6) Investigating the biological activity of the prepared nanomaterials.

(7) Study some applications for the prepared nanomaterials.

Refrences of introduction

(1) R. H. J. Hannink and A. J. Hill, Nanostructure control of materials, Woodhead Publishing Limited and CRC Press LLC, Cambridge England (2006) and references there in.

(2) M. Haruta, Catal. Today, 36 (1997) 153.

(3) Gerbericha and W. *et al*., *J.* Mech. and Phys. of Soli., 51 (2003) 979.

(4) M. Verdier, M. Niewczas, J. D. Embury, M. Nastasi and H. Kung, Mat. Resear. Soc. Sym. Proc., 77 (1998) 522.

(5) W. P. Kirk and M. A. Reed, Nanostructures and Mesoscopic Systems, New York, Academic Press, 1992.

(6) Cap-XX website www.cap-xx.com

(7) M. Koepenick, Nanovation Invasion. How real is it?. Pulp and Paper Canada.105 (1) (2004)19.

(8) P. Y. Simons, F. Dachille, Acta Cryst., 23(1967) 334.

(9) M. Latroche, L. Brohan, R. Marchand and M. Tournoux, J. Soli. Stat. Chem., 79 (1989) 78.

(10) A. Norotsky, J. C Jamieson and O. J Kleppa, Science 158 (1967) 338.

(11) H. Z. Zhang and J. F Banfield. J. Mater. Chem., 8 (1998) 2073.

(12) H. Zhang and J. F. Banfield, J. Phys. Chem., B104 (2000) 3481.

(13) E. F. Heald and C. W. Weiss, Am Min 57 (1972) 20.

(14) P. N. Kumar, K. Keizer, A. J. Burggraff, T. Okubo, H. Nagomoto and S. Morooka. Nature 48 (1992) 358.

(15) O. Carp, C. L. Huisman and A. Reller, Progress in Solid State Chemistry 32 (2004) 33, and references therein.

(16) H. A. Macleod, Thin film optical filters. 2nd ed. New York: MacMillan, 1986.

(17) P. T. Moseley and B. C. Tofield, Solid state gas sensors. Bristol: Adam Hilger; 1987.

(18) N. Savage, B. Chwieroth, A. Ginwalla, B. R. Patton, S. A. Akbar and P. K. Dutta. Sensors Actuators B17 (2001)79.

(19) M. Nabari, S. Doeuff, C. Sanchez, and J. Livage, Mater. Sci. Eng. B3 (1989) 203.

(21) J. E. Jaffe, R. Pandey, and A. B. Kunz, Phys. Rev. B 43, (1991)14030

(22) M. H. Huang, Y. Wu, H. Feick, N. Tran, E. Weber and P. D. Yang, Adv. Mater., **13** (2001) 113.

(23) K. Ghule, A. V. Ghule, B. Chen and Y. Ling, Green Chem.,8 (2006) 1034

(24) S. Fu, X. Liu, X. Zhang, Mater. Resea. Bull. 41, Issue 3, 9 (2006) 620

(25) G. Zhou, Q. Yao, X. Wang and J. C. Yu, Mater. Chem. and Phys. 98, Issues 2-3, (2006) 267.

(26) J. Karlsson, A. Roos, Solar Energy, **68** (2000) 493.

(27) L. Diaz , C.M. Liauw, M. Edge , N.S. Allen, A. McMahon, N. Rhodes J. Coll. and Inter. Sci. 287 (2005) 379.

(28) M. Feldman and P. Desrochers, Industry and Innovation 10 (2003) 1, 5.

(29) Y. M. Wang, S. W. Liu, Z. Xiu, X. B. Jiao, X. P. Cui and J. Pan, Mater. Lette. 60 (2006) 974.

(30) W. C. Bell, M. L. Myrick, J. Colloid Interface Sci. 242 (2001) 300.

(31) K. P. Velikov, G. E. Zegers, A. V. Blaaderen, Langmuir 19 (2003) 1384.

(32) L. A. Brook, P. Evans, H. A. Foster, M. E. Pemble, A. Steele, D. W. Sheel and H. M. Yates, J. Photochem. and Photobiol. A: Chemistry 187 (1) (2007) 53.

(33) G. Rajagopal, S. Maruthamuthu, S. Mohanan and N. Palaniswamy Colloids and Surfaces B: Biointerfaces 51 (2006) 107.

(34) H. Szymanowski, A. Sobczyk, M. Gazicki-Lipman, W. Jakubowski and L. Klimek, Surf. & Coat. Techno., 200 (2005) 1036.

(35) O. Yamamoto, J. Sawai and T. Sasamoto, Intern. J. Inorg. Mater., 2 (2000) 451.

(36) S. Karvinen and R. Lamminmäki, Soli. Stat. Scien. 5 (2003) 1159.

(37) Q. Sheng, S. Yuan, J. Zhang and F. Chen, Microp. and Mesop. Mater. 87 (2006) 177.

(38) J. H. Yu, S.Y. Kim, J. S. Lee, and K. H. Ahn, NanoStruct. Mater.,

12 (1999) 199.

(39) K. Okuyamaa, W. Wang, I. W. Lenggoro, Y. Terashi, T. O. Kimc, Mater. Scien. and Engineer., B 123 (2005) 194.

(40) S. H. Song, X. Wang and P. Xiao, Mater. Sci. and Eng. B 94 (2002) 40

(41) C. K. Maiti, S. K. Samanta, G. K. Dalapati, S. K. Nandi and S. Chatterjee, Microelect. Eng. 72 (2004) 253.

(42) M. Baraton and L. Merhari, J. Eur. Ceram. Soc., 24 (2004) 1399.

(43) T. Zhang, T. Oyama, S. Horikoshi, H. Hidaka, J. Zhao and N. Serpone Solar. Ener. Mater. & Solar Cells. 73 (2002) 287.

(44) R. Yuan, R. Guan, W. Shen and J. Zheng, J. Collo. and Interfa. Sci. 282 (2005) 87.

(45) H. Lachheb, E. Puzenat, A. Houas, M. Ksibi, E. Elaloui, C. Guillard and J. Herrmann, Appl. Cata. B: Envir. 39 (2002) 75.

(46) A. Houas, H. Lachheb, M. Ksibi, E. Elaloui, C. Guillard and J. Herrmann, Appl. Cata. B: Envir. 31 (2001) 145.

(47) C. H. Kwon, H. Shin, J. H. Kim, W. S. Choi and K. H. Yoon, Mater. Chem. and Phys. 86 (2004) 78.

(48) J. Hong, C. Sun, S.Yang, Y. Liu and J.Hazar. Mater. B133 (2006) 162.

(49) V.K. Gupta, R. Jain, A. Mittal, M. Mathur and S. Sikarwar, J. Coll. and Inter. Sci., 309, Issue 2,(2007)464

(50) G. Sivalingam, K. Nagaveni, M. S. Hegde and G. Madras, Appl. Cata. B: Envir.45 (2003) 23.

(51) L. Andronic and A. Duta, Thin Solid Films xx (2007) xxx.

(52) W. Baran, A. Makowski, W. Wardas, Dyes and Pigments, 76, Issue 1, (2008)226

(53) G. Madras, K. Nagaveni, G. Sivalingam and M. S. Hegde, Appl.

Cata. B: Envir. 48 (2004) 83.

(54) P. V. Messina and P. C. Schulz, J.Collo. and Interf. Sci. 299 (2006) 305.

(55) T. Yuranova, D. Laub and J. Kiwi, Cata. Today 122 (2007) 109.

(56) M. M. Mohamed, W. A. Bayoumy, M. Khairy, M. A. Mousa, Micro. and Meso. Mater. 103, Issues 1-3 (2007) 174.

(57) M. M. Mohamed, W. A. Bayoumy, M. Khairy, M. A. Mousa, Micro. and Meso. Mater. 97, Issues 1-3 (2006) 66.

(58) R. Cai , G. M. Van, P. K. Aw and K. Itoh, C. R. Chimie 9 (2006) 829

(59) T. Nguyen, H. Lee and O. Yang, Solar Ene. Mater. & Solar Cells, 90, Issues 7-8 (2006) 967.

(60) T. Tsuzuki and P. G. McCormick, Scripta mater. 44 (2001) 1731.

(61) B. Geng, X. Liu, X. Wei and S. Wang, Mater. Lette. 59 (2005) 3572.

(62) H. Zhong, J. Wang, M. Pan, S. Wang, Z. Li, W. Xu, X. Chen and W. Lu, Mater. Chem. and Phys. 97, Issues 2-3,(2006)390.

(63) G. Wang, C. Xu, G. Xu and Y. Liu, Soli. Stat. Commun., 122 (2002) 175.

(64) F. Bait, P. He, Z. Jia, X. Huang and Y. He, Mater. Lette. 59 (2005) 1687.

(65) T. Hirai, Y. Asada, J. Collo. and Interf. Sci. 284 (2005) 184.

(66) S. C. Zhang and X. G. Li, Collo. and Surf. A: Physicochem. Eng. Aspects 226 (2003) 35.

(67) H. J. Fan, R. Scholz, F. M. Kolb, M. Zacharias and U. Go¨sele, Soli. Stat. Commun. 130 (2004) 517.

(68) S. Maensiria, P. Laokul and V. Promarak, J. Cryst. Grow. 289 (2006) 102.

(69) T. Kawano and H. Imai, J. Crys. Grow. 283 (2005) 490.

(70) X. Xing, K. Zheng, H. Xu, F. Fang, H. Shen, J. Zhang, J. Zhu, C. Ye,

G. Cao, D. Sun and G. Chen, Micron 37 (2006) 370.

(71) L. Zhang, Y. Jiang, Y. Ding, M. Povey and D. York, J. Nano. Resea., 9(2006) 479.

(72) O. Yamamoto, M. Komatsu, J. Sawai and Z. Nakagawa, J. Mater. Sci.: Mater. in Med.,15 No8 (2004) 847.

(73) O. Yamamoto, Inter. J. Inorg. Mater. 3 (2001) 643.

(74) Y. J. Jang, C. Simer and T. Ohm, Mater. Resea. Bull. 41, Issue 1 (2006) 67

(75) F. Wei and D. Tao, Mater. Lette. 58 (2004) 3226.

(76) L. Wu, Y. Wu, H. Wei, Y. Shi, C. Hu, Mater. Lette. 58 (2004) 2700.

(77) N. Cordente, B. Toustou, V. Collière, C. Amiens, B. Chaudret, M. Verelst, M. Respaud and J. Broto, C. R. Acad. Sci. Paris, Chimie / Chemistry 4 (2001) 143.

(78) V. Biju and M. Abdul Khadar, Mater. Resea. Bull. 36 (2001) 21.

(79) S. Marzouk, F. Rachdi, M. Fourati and J. Bouaziz, Collo. and Surfa. A: Physicochem. Eng. Aspects 234 (2004) 109.

(80) L. A. Belyakova and A. M. Varvarin, Collo. and Surfa. A: Physicochem. and Eng. Aspects 154 (1999) 285.

(81) S. K. Parida, S. Dash, S. Patel and B. K. Mishra, Adv. in Collo. and Interf. Sci., 121, Issue 1-3 (2006) 77.

(82) L. K. Adams, D. Y. Lyon and P. J. J. Alvarez, Water Research 40 (2006) 3527.

(83) K. Y. Kim, Y. T. Choi, D. J. Seo and S. B. Park, Mater. Chem. and Phys., 88 (2004) 377.

(84) S. Eiden-Assmann, J. Widoniak and G. Maret, Collo. and Surf. A:

Physicochem. Eng. Aspects 270-271 (2005) 340

(85) B. S. Atiyeh, M. Costagliola, S. N. Hayek and S. A. Dibo, burns xxx (2006) xxx.(Agbio)

(86) K. F. Soto, A. Carrasco T. G. Powell, L. E. Murr and K. M. Garza, Mater. Sci. and Eng. C 26 (2006) 1421.

(87) S. Pal, Y. K. Tak and J. M. Song, Appl. and Environ. Microbiol., 73, No. 6(2007) 1712.

X) L. Diaz , C.M. Liauw, M. Edge , N.S. Allen, A. McMahon, N. Rhodes J. Coll. and Inter. Sci. 287 (2005) 379.